6th ECCOMAS Conference on Smart Structures and Materials
SMART2013
Politecnico di Torino, 24-26 June 2013
E. Carrera, F. Miglioretti and M. Petrolo (Editors)
www.smart2013.com

IDENTIFICATION OF SEMI-RIGID JOINTS IN FRAME STRUCTURES

Andrzej Świercz[*†a], **Przemysław Kołakowski**[†b], **Jan Holnicki-Szulc**[*c], **Dorota Olkowicz**[*d]

[*] Polish Academy of Sciences
Institute of Fundamental Technological Research
ul. Pawińskiego 5B
02-106 Warsaw, Poland
e-mails: [a] aswiercz@ippt.pan.pl, [c] holnicki@ippt.pan.pl, [d] dolkow@ippt.pan.pl,
web page: http://smart.ippt.gov.pl

[†] Adaptronica sp. z o.o., R&D company
05-092 Łomianki, Poland
e-mails: [a]aswiercz@adaptronica.pl, [b]plolak@adaptronica.pl, web page: http://www.adaptronica.pl

Key words: Frame structures, Semi-rigid joints, Inverse problem, SHM.

Summary. *This study presents the numerical analysis and experimental tests of a planar frame structure with semi-rigid joints. Based on structural responses the identification of nodal parameters is performed.*

1. INTRODUCTION

A typical analysis of frame structures assumes that the element connections are idealized i.e. rigid or pin-joined. In real systems though, the performance of such connections can be represented by the so-called semi-rigid joints. The semi-rigid joint covers the whole range of intermediate characteristics between the two idealized ones mentioned above. The structural design code [1] provides guidelines for engineers, however they do not widely apply probably due to difficulties of assessment and/or insufficient guidelines of such connections.

This work is aimed at identification of the semi-rigid joints in frame structures i.e. determination of their positions and characteristics. For a structure under load, a modification of the nodal connection influences structural displacements and internal forces. They are calculated using a constitutive law, which relates the nodal bending moment and the relative rotation of the connected elements. In this work the process of the updating of structural responses is performed using the Virtual Distortion Method (VDM). An extensive discussion of this approach for static and dynamic problems can be found in [2, 3]. On the individual structural elements, some deformations are imposed. They are called virtual distortions and depend on actual loading and modification of element connections. This method allows for computation of analytical gradients and is useful for gradient-based optimization procedures.

It should be noted, the presented approach is based on finite element method and qualitatively different than methods utilizing a dedicated local stiffness matrix for element flexible nodal connections, cf. [4, 5].

2. MODELLING OF THE SEMI-RIGID JOINTS

2.1 Semi-rigid connections

In general, a joint may be classified as rigid, pinned or semi-rigid according to rotational stiffness. A mathematical model of a semi-rigid connection can be characterised by moment-rotation or curvature-rotation characteristics. In this study, the connection between a finite element and a node is modelled by a linear rotational spring as shown in Fig. 1, where M denotes the applied moment associated with the angle of rotation $\overset{0}{\varphi}$ of the spring. The constitutive

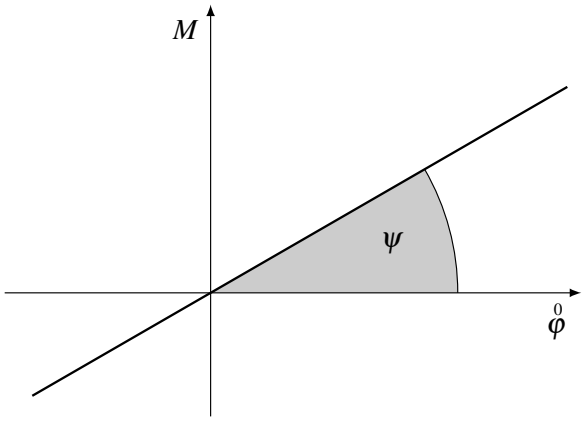

Figure 1. Moment-curvature characteristic for a rotational spring.

relation can be written in the simple form:

$$M = \overset{0}{\varphi} \tan\psi = \overset{0}{\varphi}\, S. \tag{1}$$

In the Eq. (1), the parameter ψ determine the rotational stiffness S of the spring. In the case of $\psi = 0$ (and $S = 0$) the spring is not capable to carry the moment and this case is used for modelling of pinned connections in beam finite elements. Another extreme case of $\psi = \frac{\pi}{2}$ (and $S \to \infty$) models the rigid connection, however Eq. (1) is not useful for modelling of a very stiff connection. For such cases Eq. (1) can be rewritten as:

$$\overset{0}{\varphi} = M \tan\left(\frac{\pi}{2} - \psi\right) = MP, \tag{2}$$

where $P = \frac{1}{S}$ denotes the compliance of the spring. Thus, the case of $\psi = \frac{\pi}{2}$ leads to $P = 0$. The springs with relatively low compliance will be used for modelling of nodal connections with relatively high rotational stiffness.

2.2 The Euler beam finite element – remarks

Let us consider a beam finite element with length of l and bending stiffness EJ. Next, initial nodal rotations $\overset{0}{\varphi}{}^{(i)}$ are applied in local nodes (1) and (2) as presented in Fig. 2, where the parameter ξ denotes dimensionless coordinate expressed by the relation:

$$\xi = \frac{2x}{l} - 1, \qquad x \in \langle 0, l \rangle \qquad \text{and} \qquad \xi \in \langle -1, 1 \rangle \tag{3}$$

Thus, the curvatures $\overset{0}{\kappa}{}^{(i)}$ in local nodes (1) and (2) caused by nodal rotation $\overset{0}{\varphi}{}^{(i)}$ can be ex-

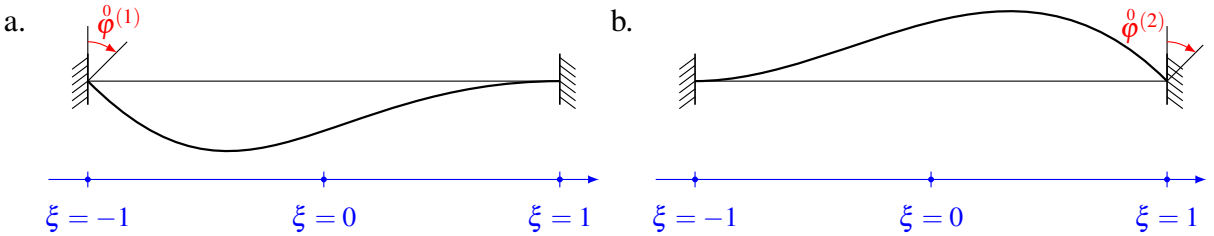

Figure 2. Deflection lines of a beam finite element caused by introduction of initial rotations: a. in node (1), b. in node (2).

pressed by the equation:

$$\overset{0}{\kappa}{}^{(i)}\left(\xi^{(i)}\right) = \frac{M^{(i)}\left(\xi^{(i)}\right)}{EJ} = \frac{4}{l}\,\overset{0}{\varphi}{}^{(i)} = \zeta\,\overset{0}{\varphi}{}^{(i)}, \tag{4}$$

where $i = 1, 2$ for local node (1) and (2), respectively, while the parameter $\zeta = \frac{4}{l}$.

In further considerations, the nodal rotation $\overset{0}{\varphi}$ is named the *angular virtual distortion* and used for modelling of semi-rigid joints. The behaviour of such connections are realized by imposing the virtual distortion $\overset{0}{\varphi}$ on a local node of a finite element. Let us note, that according to Eq. (4), the *curvature virtual distortion* $\overset{0}{\kappa}$ can be equivalently applied. For any angular virtual distortion, the corresponding nodal forces (so-called *compensating loads*) can be straightforwardly determined by multiplication of a local stiffness matrix of a finite element and the vector of nodal displacements, which are equal to zero except for the coordinate corresponding to the imposed nodal rotation $\overset{0}{\varphi}$.

3. VDM-based model updating approach

3.1 Curvature influence matrix

Now, let us consider a beam structure with a set of nodal connections to be modelled as non-rigid. Initially, on the rigid connections we impose consecutively the *unit curvature distortions*,

cf. Eq. (4). As a result, we get the *distortion states*, which have to be independently solved and the nodal curvatures saved for a set of modelled nodal connections in columns of matrix $B_{\alpha\beta}$. In this way, we get the *curvature influence matrix* $B_{\alpha\beta}$ which is used for the updating of nodal curvatures caused by introduction of the virtual distortions $\overset{0}{\kappa}_\alpha$ (or $\overset{0}{\varphi}_\alpha$) according to the following formula:

$$\kappa_\alpha = \overset{\mathrm{L}}{\kappa}_\alpha + B_{\alpha\beta}\overset{0}{\kappa}_\beta - \overset{0}{\kappa}_\alpha, \tag{5}$$

where $\overset{\mathrm{L}}{\kappa}_\alpha$ is a vector of nodal curvatures obtained for the *original structure* (i.e. without any imposed virtual distortion) under determined load. In Eq. (5), the term $B_{\alpha\beta}\overset{0}{\kappa}_\beta$ itself is equivalent to curvature responses obtained for compensating loads and does not introduce any rotational discontinuities in nodal connections. To this end the nodal curvatures $\overset{0}{\kappa}_\alpha$ which correspond to the imposed angular virtual distortions $\overset{0}{\varphi}_\alpha$, have to be additionally taken into account.

3.2 Modelling of semi-rigid joints by the VDM approach

Now, we assume the beam finite elements are connected to nodes using linear rotational springs. For further considerations it is convenient to express the spring characteristics in a space of curvature-rotation, i.e. refer the bending moment M_α of an finite element to the bending stiffness $E_{\underline{\alpha}}J_{\underline{\alpha}}$ of this element. The indices run over modelled nodal connections and there is no summation over underlined indices. Two examples of such characteristics are presented in Fig. 3a. The first characteristic – line (a) determined by Θ_α – models the compliance of a nodal connection, while the second – line (b) determined by ψ_α – models the stiffness of a nodal connection. Analogously to Eq. (1) and Eq. (2) we can rewrite the constitutive law of the rotational spring:

$$\kappa_\alpha = \overset{0}{\varphi}_{\underline{\alpha}} \tan\psi_{\underline{\alpha}} = \overset{0}{\varphi}_{\underline{\alpha}}\, s_{\underline{\alpha}} \qquad \text{for} \qquad 0 \le \mu_\alpha \le \frac{1}{2} \qquad \text{and} \qquad \psi_\alpha = \frac{\pi}{2}\mu_\alpha, \tag{6}$$

$$\overset{0}{\varphi}_\alpha = \kappa_{\underline{\alpha}} \tan\Theta_{\underline{\alpha}} = \kappa_{\underline{\alpha}}\, p_{\underline{\alpha}} \qquad \text{for} \qquad \frac{1}{2} < \mu_\alpha \le 1 \qquad \text{and} \qquad \Theta_\alpha = \frac{\pi}{2}\left(1-\mu_\alpha\right). \tag{7}$$

In Eq. (6) and (7), a dimensionless coefficient $\mu_\alpha \in \langle 0,1\rangle$ is introduced. For a rigid joint, i.e. $\mu_\alpha = 1$, the compliance of the nodal connection is equal to $s_\alpha = \tan(0) = 0$, while rotational stiffness yields $p_\alpha = \tan\left(\frac{\pi}{2}\right) \to \infty$. In the second extreme case, for $\mu_\alpha = 0$ (pinned joint), the compliance of the nodal connection is singular i.e. $s_\alpha = \tan(\frac{\pi}{2}) \to \infty$, while rotational stiffness yields $p_\alpha = \tan(0) = 0$. To avoid singularities in these extreme cases, the modelling is divided into two cases, cf. Eq. (6) and (7). For the first case, i.e. $\mu_\alpha \in \left\langle 0, \frac{1}{2}\right\rangle$, semi-rigid joints are modelled using parameter $\psi_\alpha \in \left\langle 0, \frac{\pi}{4}\right\rangle$ (rotational stiffness modification), whereas for the second case, i.e. $\mu_\alpha \in \left(\frac{1}{2}, 1\right\rangle$, the joints are modelled using parameter $\Theta_\alpha \in \left\langle 0, \frac{\pi}{4}\right)$ (rotational compliance modification).

Let us rewrite Eq. (4) for all modelled nodal connections:

$$\overset{0}{\varphi}_\alpha = \frac{1}{4} l_{\underline{\alpha}}\, \overset{0}{\kappa}_{\underline{\alpha}} = \zeta_{\underline{\alpha}}\, \overset{0}{\kappa}_{\underline{\alpha}} \tag{8}$$

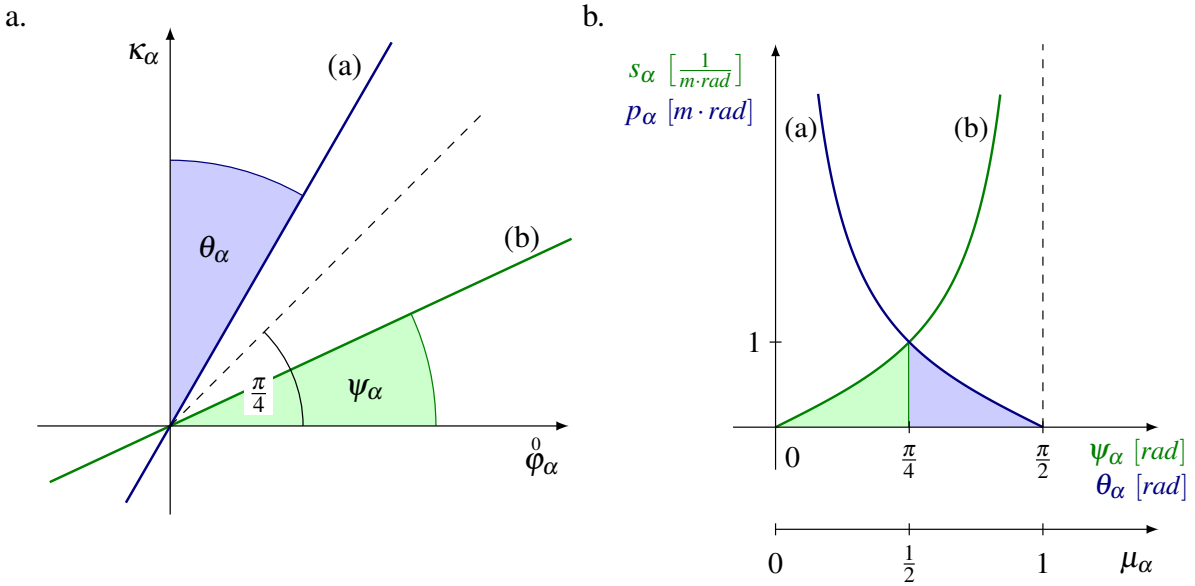

Figure 3. a. Examples of linear curvature-rotational characteristics for a rotational spring. b. Curves of the rotational compliance (a) and rotational stiffness (b).

Substituting Eq. (8) into Eq. (6) and (7) and next using Eq. (5) we get equations for the two above-mentioned cases:

$$(\delta_{\underline{\alpha}\beta}\zeta_{\underline{\alpha}}s_{\underline{\alpha}}(\mu_\alpha) + \delta_{\alpha\beta} - B_{\alpha\beta})\overset{0}{\kappa}_\beta = \overset{\mathrm{L}}{\kappa}_\alpha \qquad \text{for} \qquad 0 \le \mu_\alpha \le \frac{1}{2}, \tag{9}$$

$$(\delta_{\underline{\alpha}\beta}\zeta_{\underline{\alpha}} + p_{\underline{\alpha}}(\mu_\alpha)\,(\delta_{\underline{\alpha}\beta} - B_{\underline{\alpha}\beta}))\overset{0}{\kappa}_\beta = p_{\underline{\alpha}}(\mu_\alpha)\overset{\mathrm{L}}{\kappa}_{\underline{\alpha}} \qquad \text{for} \qquad \frac{1}{2} < \mu_\alpha \le 1. \tag{10}$$

Equations (9) and (10) allows for computation of the curvature virtual distortions $\overset{0}{\kappa}_\alpha$ for given nodal modifications coefficient μ_α. Let us notice, Eq. (9) and (10) are valid for the range $0 \le \mu_\alpha \le 1$, but for computational reasons it is convenient to define two intervals (cf. Fig. 3b). Anyway, we can transform Eq. (9) and (10) into a single equation:

$$[\delta_{\underline{\alpha}\beta}\zeta_{\underline{\alpha}}s_{\underline{\alpha}}(\mu_\alpha) + p_{\underline{\alpha}}(\mu_\alpha)\,(\delta_{\underline{\alpha}\beta} - B_{\underline{\alpha}\beta})]\overset{0}{\kappa}_\beta = p_{\underline{\alpha}}(\mu_\alpha)\overset{\mathrm{L}}{\kappa}_{\underline{\alpha}} \tag{11}$$

with additional restrictions for $s_\alpha(\mu_\alpha)$ and $p_\alpha(\mu_\alpha)$:

$$s_\alpha(\mu_\alpha) = \begin{cases} \tan\left(\frac{\pi}{2}\mu_\alpha\right) & \text{for} \quad 0 \le \mu_\alpha \le \frac{1}{2}, \\ 1 & \text{for} \quad \frac{1}{2} < \mu_\alpha \le 1, \end{cases} \tag{12}$$

$$p_\alpha(\mu_\alpha) = \begin{cases} 1 & \text{for} \quad 0 \le \mu_\alpha \le \frac{1}{2}, \\ \tan\left(\frac{\pi}{2}\,(1-\mu_\alpha)\right) & \text{for} \quad \frac{1}{2} < \mu_\alpha \le 1. \end{cases} \tag{13}$$

Furthermore, Eq. (11) can be written in the simple form:

$$A_{\alpha\beta}\,\overset{0}{\kappa}_{\beta} = \overset{\mathrm{L}}{b}_{\alpha}, \tag{14}$$

where: $A_{\alpha\beta} = \delta_{\underline{\alpha}\beta}\zeta_{\underline{\alpha}}s_{\underline{\alpha}} + p_{\underline{\alpha}}\left(\delta_{\underline{\alpha}\beta} - B_{\underline{\alpha}\beta}\right)$ and $\overset{\mathrm{L}}{b}_{\alpha} = p_{\underline{\alpha}}\overset{\mathrm{L}}{\kappa}_{\underline{\alpha}}$. The first term of the matrix $A_{\alpha\beta}$ constitutes a diagonal matrix with elements $\zeta_{\underline{\alpha}}s_{\underline{\alpha}}$ and becomes zeros for $\mu_{\alpha} = 0_{\alpha}$. On the other hand, for the case of all rigid nodal connections ($\mu_{\alpha} = 1_{\alpha}$), the first part remains a diagonal matrix, the second part of the matrix $A_{\alpha\beta}$, i.e. $p_{\underline{\alpha}}\left(\delta_{\underline{\alpha}\beta} - B_{\underline{\alpha}\beta}\right)$, is a zero matrix, and the right-hand side of Eq. (14) is a zero vector, which results in $\overset{0}{\kappa}_{\alpha} = 0_{\alpha}$.

3.3 Dynamics

For dynamic problems, the curvature virtual distortions $\overset{0}{\kappa}_{\alpha}(t)$ and the curvature influence matrix $B_{\alpha\beta}(t)$ are time-dependent. The updated nodal curvatures are computed using the formula analogous to Eq. (5):

$$\kappa_{\alpha}(t) = \overset{\mathrm{L}}{\kappa}_{\alpha}(t) + \sum_{\tau=0}^{t} B_{\alpha\beta}(t-\tau)\,\overset{0}{\kappa}_{\beta}(\tau) - \overset{0}{\kappa}_{\alpha}(t) \tag{15}$$

In Eq. (15) there appears a convolution of the curvature influence matrix $B_{\alpha\beta}$ and the virtual distortions $\overset{0}{\kappa}_{\alpha}$. The influence matrix $B_{\alpha\beta}$ is computed by applying the compensating forces (obtained as for the static analysis) corresponding to the unit curvature virtual distortions at the first step of dynamic analysis with zero initial conditions. The relationships (6) and (7) are valid here as well, assuming, that the nodal curvatures κ_{α} and the angular virtual distortion $\overset{0}{\varphi}_{\alpha}$ are also time-dependent. With this in mind, performing algebraic transformations we get the formula for determining the virtual distortions $\overset{0}{\kappa}_{\alpha}$ (analogous to Eq. 14):

$$A_{\alpha\beta}\,\overset{0}{\kappa}_{\beta}(t) = \overset{\mathrm{L}}{b}_{\alpha}(t), \tag{16}$$

where the left-hand side matrix $A_{\alpha\beta}$ and the right-hand side vector $\overset{\mathrm{L}}{b}_{\alpha}(t)$ are expressed by the following relationships:

$$A_{\alpha\beta} = \delta_{\underline{\alpha}\beta}\zeta_{\underline{\alpha}}s_{\underline{\alpha}} + p_{\underline{\alpha}}\left(\delta_{\underline{\alpha}\beta} - B_{\underline{\alpha}\beta}(0)\right), \tag{17}$$

$$\overset{\mathrm{L}}{b}_{\alpha}(t) = \begin{cases} p_{\underline{\alpha}}\overset{\mathrm{L}}{\kappa}_{\underline{\alpha}}(0) & \text{for} \quad t = 0, \\ p_{\underline{\alpha}}\left[\overset{\mathrm{L}}{\kappa}_{\underline{\alpha}}(t) - \sum_{\tau=0}^{t-1} B_{\underline{\alpha}\beta}(t-\tau)\,\overset{0}{\kappa}_{\beta}(\tau)\right] & \text{for} \quad t > 0. \end{cases} \tag{18}$$

Equation (16) is iteratively solved for each time step t. Fortunately, the left-hand side matrix $A_{\alpha\beta}$ is computed only once, nevertheless the right-hand side vector $\overset{\mathrm{L}}{b}_{\alpha}(t)$ has to be calculated for each time step t.

Let us notice, that for the generalized influence matrix $\hat{B}_{i\beta}$ whose columns contain other responses than curvatures (e.g. nodal displacements $u_i(t)$ or accelerations), we are able to calculate other responses we are interested in:

$$u_i(t) = \overset{\mathrm{L}}{u}_i(t) + \sum_{\tau=0}^{t} \hat{B}_{i\alpha}(t-\tau)\, \overset{0}{\kappa}_\alpha(\tau), \tag{19}$$

using the previously determined curvature virtual distortions $\overset{0}{\kappa}_\alpha(t)$ from Eq. (16).

3.4 Gradient-based identification of the semi-rigid joints

The aim of this section is to present a procedure for an identification of the nodal modification coefficients μ_α based on structural responses. Let us assume, there are known measured responses for the original structure (rigid connections), e.g. nodal accelerations $\ddot{u}_i(t)$, and the modified structure (with semi-rigid joints) $\ddot{u}_i^M(t)$. The responses can be simulated numerically using a model well-matched with experiments. Based on those responses the following objective function is proposed:

$$F(\mu_\alpha) = \sum_i \frac{\sum\limits_t \left(\ddot{u}_i(\mu_\alpha, t) - \ddot{u}_i^M(t)\right)^2}{\sum\limits_t \left(\ddot{u}_i^M(t)\right)^2}, \tag{20}$$

where $\ddot{u}_i(\mu_\alpha, t)$ is the vector of the responses modelled by the virtual distortions $\overset{0}{\kappa}_\alpha(t)$ and μ_α is the vector of optimization variables. The vector μ_α can be iteratively determined using e.g. the steepest descent method:

$$\mu_\alpha^{k+1} = \mu_\alpha^k - \Delta F^k \frac{F_{,\alpha}}{||F_{,\alpha}||^2}, \tag{21}$$

where the upper superscript $k+1$ denotes current iteration and k denotes previous iteration. The parameter Δ is a constant from the interval of $(0.1, 0.3)$ or can be iteratively determined (sub-optimization task) for each iteration k using the line search method. In Eq. (21) F^k is the value of the objective function in the k-th iteration, whereas $F_{,\gamma}$ is the gradient of the objective function. This gradient can be computed using the following relation:

$$F_{,\alpha} = \frac{\partial F}{\partial \mu_\alpha} = \frac{\partial F}{\partial \ddot{u}_i} \frac{\partial \ddot{u}_i}{\partial \overset{0}{\kappa}_\gamma} \frac{\partial \overset{0}{\kappa}_\gamma}{\partial \mu_\alpha}. \tag{22}$$

The respective gradients can be determined in the following way:

- the gradient objective function F with respect of $\ddot{u}_i$ – by differentiation of Eq. (20):

$$F_{,i} = \frac{\partial F}{\partial \ddot{u}_i} = 2\, \frac{\sum\limits_t \left(\ddot{u}_i(t) - \ddot{u}_i^M(t)\right)}{\sum\limits_t \left(\ddot{u}_i^M(t)\right)^2}; \tag{23}$$

- the gradient of modelled accelerations $\ddot{u}_i$ with respect of the curvature virtual distortions $\overset{0}{\kappa}_\gamma$ – by differentiation of Eq. (19):

$$\ddot{u}_{i,\gamma}(t) = \frac{\partial \ddot{u}_i}{\partial \overset{0}{\kappa}_\gamma} = \hat{B}_{i\gamma}(t); \tag{24}$$

- the gradient of the curvature virtual distortions $\overset{0}{\kappa}_\gamma$ with respect to the design parameters μ_α – by differentiation of Eq. (16):

$$A_{\gamma\beta}\overset{0}{\kappa}_{\beta,\alpha}(t) = p_{\underline{\gamma},\alpha}\,\kappa_{\underline{\gamma}}(t) - \delta_{\underline{\gamma}\beta}\,\zeta_{\underline{\gamma}}\,s_{\underline{\gamma},\alpha}\overset{0}{\kappa}_\beta(t) + p_{\underline{\gamma}}\left(\sum_{\tau=0}^{t-1} B_{\underline{\gamma}\beta}(t-\tau)\,\overset{0}{\kappa}_{\beta,\alpha}(\tau)\right). \tag{25}$$

4. NUMERICAL EXAMPLE

As a numerical example let us consider the frame structure shown in Fig. 4 and consisting of 11 steel elements with length of 51cm, rectangular-shaped cross sections (80mm by 8mm) and density $\varrho = 7850\ \frac{\text{kg}}{\text{m}^3}$. The excitation load is applied to node 6 and time-dependency of the force is presented in Fig. 5.

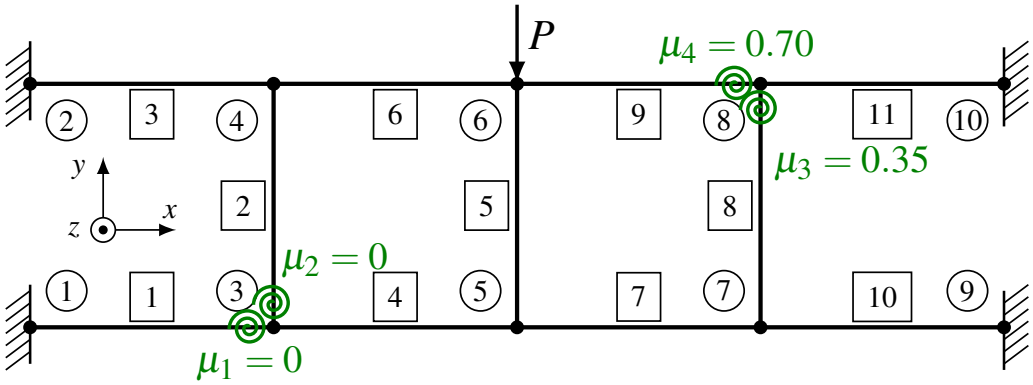

Figure 4. Tested frame structure with marked nodal modifications.

In the first step, the dynamic analysis was performed (Newmark method) for the loaded original structure, i.e. with all rigid nodal connections and for nodes 3–8 accelerations in the y–direction were stored. The curvature and generalized (associated with accelerations in the above mentioned nodes) influence matrices were generated. The following nodal modification coefficients were assumed: $\mu_1 = 0$, $\mu_2 = 0$, $\mu_3 = 0.35$, $\mu_4 = 0.70$ (cf. Fig. 4). Finally, the accelerations were recalculated (for nodes 3–8, y–direction). A comparison of the selected accelerations obtained at node 7 for the original and modified structure is shown in Fig. 6.

In the last step, the optimization procedure discussed in subsection 3.4 was applied. The objective function was defined using the computed accelerations in six nodes. In Fig. 7 (top figure) we can follow a variation of the optimization process, where the objective function was referred to initial value in each iteration, i.e. $\frac{F^i}{F^1}$, in the logarithmic scale. In the lower figure, the correctly identified nodal modification coefficients in each iteration are presented.

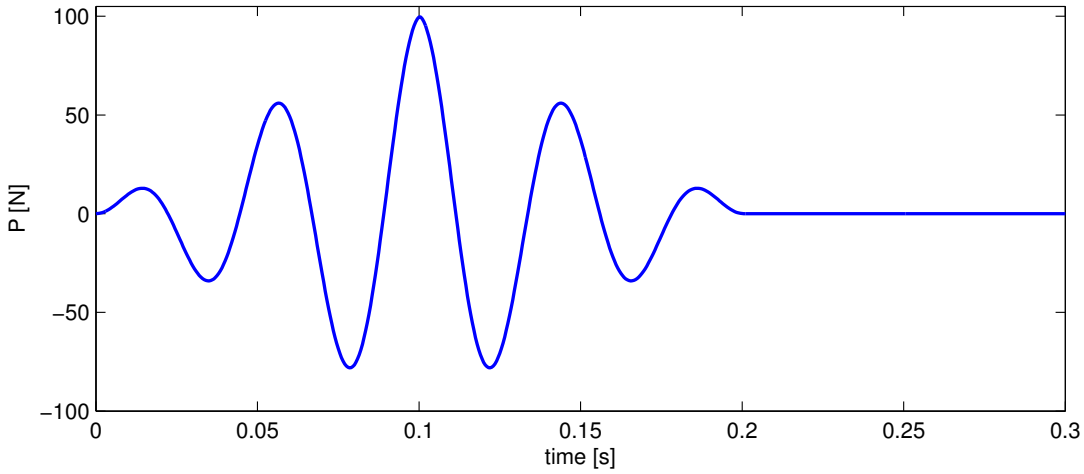

Figure 5. The load function applied to node 6.

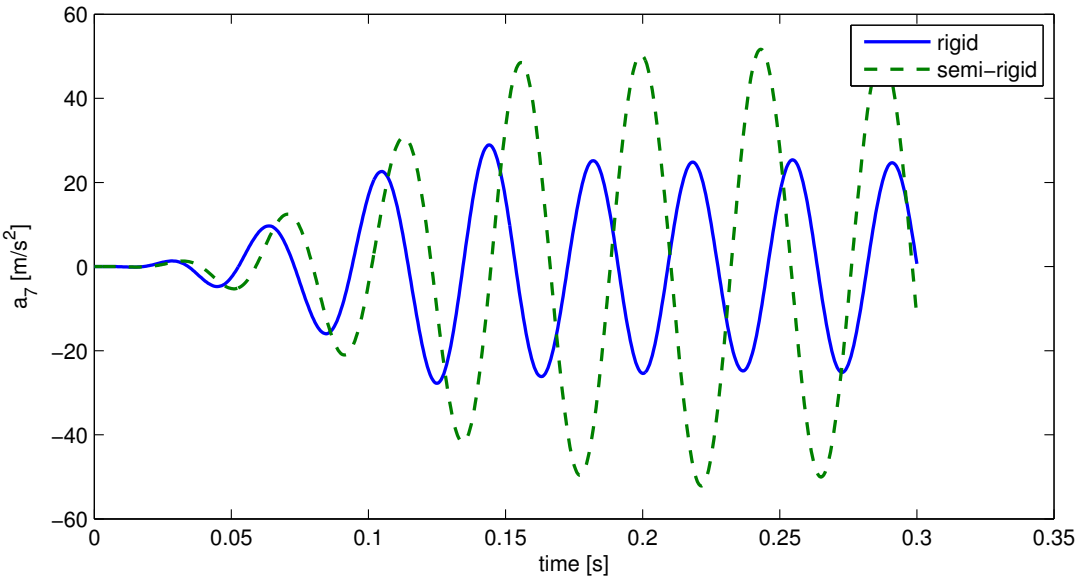

Figure 6. The accelerations computed at node 7 for original and modified structure.

5. EXPERIMENTAL TESTS

A preliminary laboratory test aimed at the identification of semi-rigid joints was performed. In Fig. 8 and Fig. 9, the experimental stand with some details is shown. The investigated structure, on which the numerical simulations were performed and presented in the previous section, consists of 11 steel elements and six changeable nodes. It is designed for easy replacement of the element connections to the nodes: fully rigid, pin-joined (cf. Fig. 9a,b) or semi-rigid. First, the structure with the rigid nodal connections was subjected to time-dependent excitation (cf. Fig. 10, continuous curve) applied at node 7 (cf. Fig. 4). The excitation signal was produced by

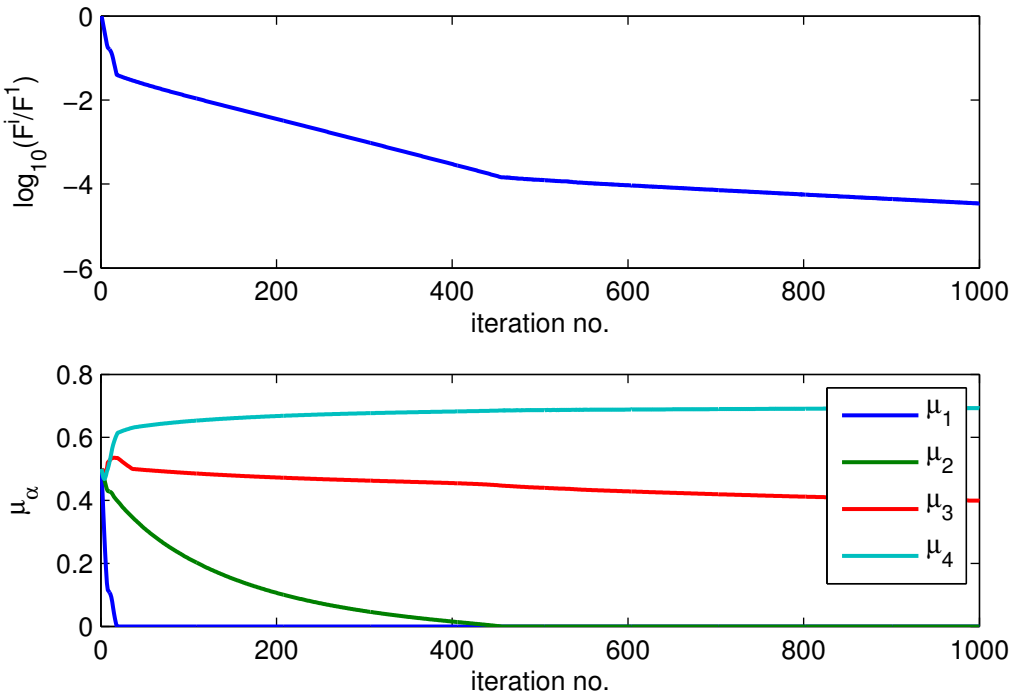

Figure 7. The values of the objective function during optimization process (top) and identified modification coefficients (bottom).

a function generator and then amplified transferred to the exciter. Next, the rigid connections at node 3 was replaced by pinned connections and the loading procedure was repeated as for original structure. The measured load is shown in Fig. 10 and marked as the dashed curve. In this way, due to different interactions between the exciter and the original and modified structure, the obtained loading functions are significantly different. For this reason, the identification procedure can not be applied for this case, since the presented optimization approach requires the same loading for the original and modified structure.

6. CONCLUSIONS

This study explores the modelling and identification of semi-rigid nodal connections in 2D frame structures based on Bernoulli's beam theory and finite element method without modification of a local element stiffness matrix. Instead, for such connections, the virtual curvature distortions field, associated with modification coefficients and supposed to implement the constitutive relationship (analogous to the linear rotational spring), is imposed. The basis for calculating of the updated nodal curvatures (or generalized responses) of finite elements for the modified structure is the curvature influence matrix (or the generalized influence matrix). This approach allows for computation of analytical gradients of the virtual distortions with respect to the modification coefficients. Therefore, it is useful for solving the gradient-based optimization problems aimed at determination of the parameters for the nodal semi-rigid connections.

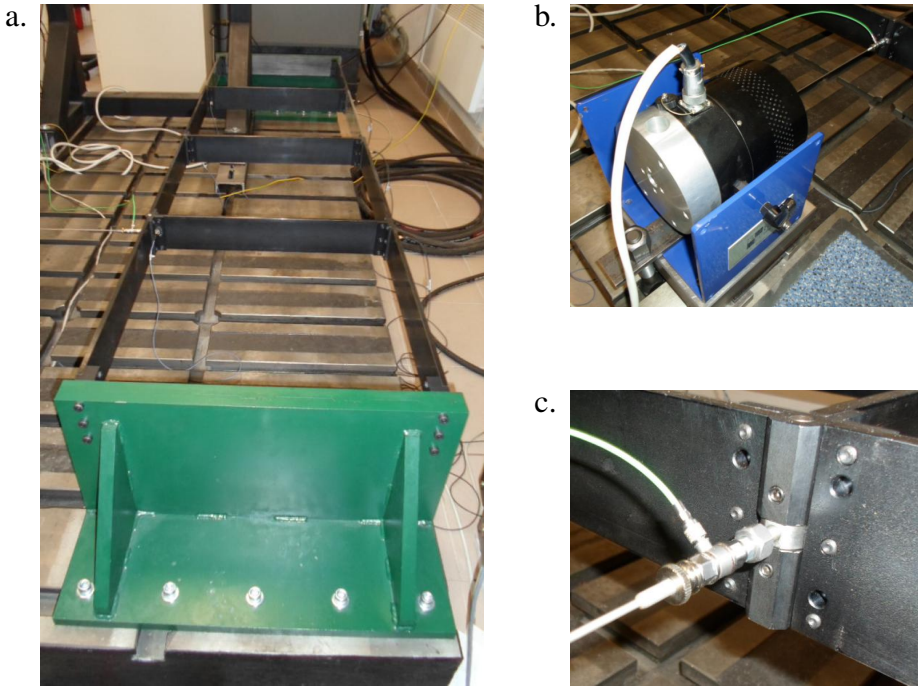

Figure 8. The tested frame structure: a. general view, b. electromagnetic exciter, c. details of the loading of a node with force sensor installed.

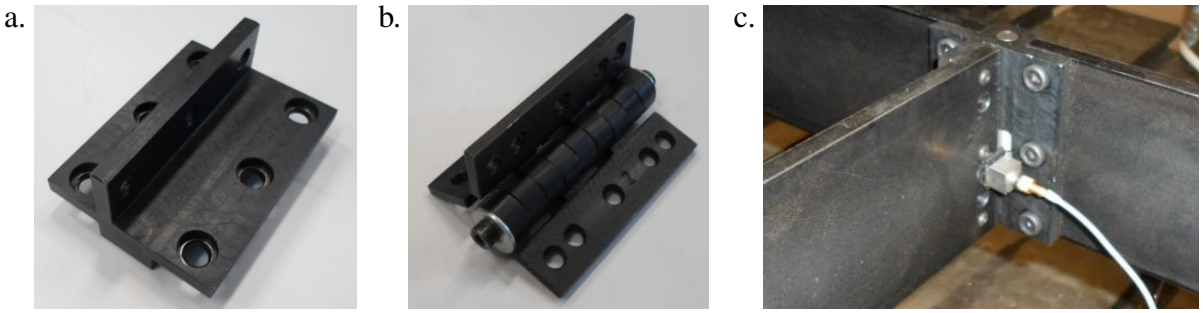

Figure 9. Detailed view of the nodes: a. rigid node, b. pinned node, c. mounted rigid node with an installed accelerometer.

The objective function is expressed in terms of responses obtained for the original and modified structure under the same load.

In this paper, a numerical example of identification of the nodal modification coefficients for the simple frame structure was successfully performed. In the laboratory test, the obtained structural excitations for the original and modified structure were substantially different. The further study will be concentrated on the application of load with the same characteristics.

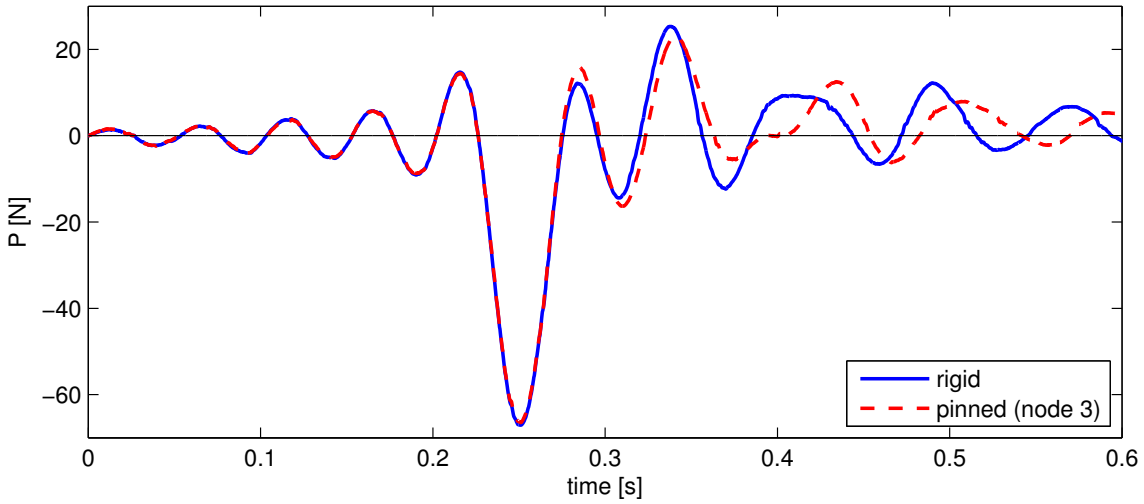

Figure 10. A comparison of the measured loading for the original and modified structure.

Acknowledgement

The authors gratefully acknowledge financial support through the FP7 EU project Smart-Nest (PIAPP-GA-2011-28499) and the Polish National Science Center (NCN) under Decision No. 0494/B/T02/2011/40.

References

[1] EN 1993-1-8:2005 *Eurocode 3: Design of steel structures – Part 1-8: Design of joints.*

[2] P. Kołakowski, *Damage Identification by the Static Virtual Distortion Method*, Engineering Transactions, vol. 52, 2004.

[3] P. Kołakowski, T. Zieliński and J. Holnicki-Szulc, *Damage identification by Dynamic Virtual Distortion Method*, Journal of Intelligent Material Systems and Structures, vol. 15, pp. 479-494, 2004.

[4] G.R. Monforton and T.S. Wu , *Matrix analysis of semi-rigidly connected steel frames*, Journal of the structural Division, ASCE, 89(6), pp. 13-42, 1963.

[5] A. Csébfalvi, *Optimal design of frame structures with semi-rigid joints*, Periodica Polytechnica Civil Engineering, vol. 51/1, pp. 9-15, doi: 10.3311/pp.ci.2007-1.02, 2007.